Published in: ACS Applied Energy Materials (2019), vol. 2, n°5, pp. 3035-3041
DOI: 10.1021/acsaem.9b00443
Status: Postprint (Author's version)

POLYMERS BEARING CATECHOL PENDANTS AS UNIVERSAL HOSTS FOR AQUEOUS RECHARGEABLE H^+, LI-ION, AND POST-LI-ION (MONO-, DI-, AND TRIVALENT) BATTERIES

Nagaraj Patil [a], Andreas Mavrandonakis [a], Christine Jérôme [b], Christophe Detrembleur [b], Jesus Palma [a], and Rebeca Marcilla* [a]

[a] *Electrochemical Processes Unit, IMDEA Energy Institute, Avenida Ramó n de la Sagra 3, 28935 Móstoles, Spain*
[b] *Centre for Education and Research on Macromolecules (CERM), CESAM Research Unit, Department of Chemistry, University of Liège, Allée de la Chimie B6A, 4000 Liège, Belgium*

Keywords: aqueous battery, multivalent battery, organic electrode material, redox-active polymer, catechol polymer, catecholato–metal cation complex, electrochemistry, density functional theory

Abstract

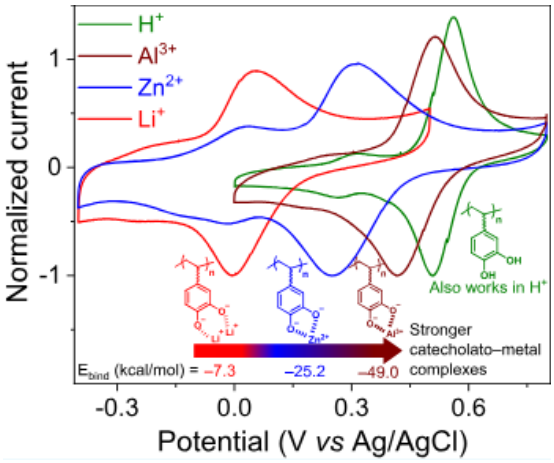

Organic electrode materials capable of reversible coordination/uncoordination of both mono- and multivalent ions in aqueous electrolytes are desired to develop safe, sustainable, and cost-effective water-based batteries. Here, we demonstrate the universality of bioinspired redox-active polymers bearing catechol pendants to reversibly coordinate/uncoordinate numerous cations including H^+ and Li^+ to Zn^{2+} and Al^{3+} with fast kinetics and ultralong cyclability. This unprecedented versatility is based on a catecholato–metal cation complex ($Cat^{2-}(mM^{n+})$) charge storage mechanism that dictates the overall electrochemistry: formation of stronger complexes in $M^+ < M^{2+} < M^{3+}$ order resulted in a huge redox potential increment that might be used to tune the operating voltage of the battery.

Published in: ACS Applied Energy Materials (2019), vol. 2, n°5, pp. 3035-3041
DOI: 10.1021/acsaem.9b00443
Status: Postprint (Author's version)

Over the past decade, aqueous rechargeable mono- (Li^+, Na^+, K^+) (1) and multivalent (Zn^{2+}, Mg^{2+}, Ca^{2+}, Al^{3+}) (2,3) ion batteries have been gathering increasing attention owing to their safety, low-cost, ecofriendly, and sustainability aspects, which are crucial for large-scale applications. (4−6) Although a plethora of inorganic intercalation compounds have been successfully applied as electrode materials in lithium-ion batteries (LIBs), their direct translation into the post-lithium-ion battery (PLIB) technologies resulted in limited success due to the constrained crystallographic lattice of classical inorganic intercalation materials. (2) Specifically, the cell performances of these PLIBs are penalized by slow kinetics, low round-trip efficiency, and unstable cycling because of large cation size, significant volume changes upon intercalation/deintercalation, and strong electrostatic interactions between the highly charged ions and the host inorganic framework. (2,3)

On the contrary, their organic counterparts, in particular, redox-active polymers (RAPs), are anticipated to show their preeminence in the PLIB era, owing to their interesting intrinsic characteristics such as the presence of "large voids" and "soft" structure that endow transport pathways for large and highly charged cations with negligible volume changes during oxidation/reduction reaction. (7−10) Among a vast variety of RAPs, carbonyl-based RAPs (e.g., carboxylates, imides, and quinones, etc.) (11) have demonstrated suitability as high-performance electrodes in PLIBs due to their potential compatibility with PLIB chemistries. Contrary to inorganic materials that store energy through an intercalation/deintercalation mechanism, these carbonyl-based RAPs store charge through a reversible "ion-coordination" mechanism, where the cations of interest coordinate to the negatively charged enolate functionality upon electrochemical reduction and uncoordinate reversibly during the reverse oxidation. (12−14) This charge storage mechanism dictates the overall electrochemical performance of the device, manifested by the strength of the enolate–cation interactions. (15) Interestingly, most of the state-of-the-art carbonyl-RAPs for PLIB are based on *p*-quinones (vide supra), and only recently, *o*-quinones have emerged as more attractive than their para-counterparts for multivalent batteries. (13,16−18) This is due to their higher discharge potential, improved reversibility, (19−21) and, most importantly, suitably located enolates (1,2-positions) able to create a conducive environment for multivalent ions coordination. (13,16,18)

In this letter, we demonstrate the universality of RAPs bearing catechol pendants to reversibly coordinate/uncoordinate numerous cations, including H^+, Li^+, Na^+, K^+, Ca^{2+}, Mg^{2+}, Zn^{2+}, Ce^{3+}, and Al^{3+}, that can be leveraged in aqueous rechargeable batteries with different features. We have chosen catechol as the bioinspired redox core because of its strong, yet reversible, promiscuous coordination (covalent with H^+) (22) complex formation with various mono- and multivalent cations (Li^+, Zn^{2+}, and Al^{3+}, etc.). (8,23) Formation of such complexes is ubiquitous to many natural systems, playing a vital role in numerous biochemical functions, such as biological energy transductions, Fe^{3+} sequestration and uptake in microbial siderophores, and adhesion and cross-linking of mussel foot protein, to mention only a few. (23) It is also revealed here how, besides macromolecular engineering of the RAPs, the nature of the electroneutralizing cations significantly affects their redox potentials and rate capabilities, benefiting from the catecholato–cation complex charge storage mechanism ($Cat^{2-}(mM^{n+})$, where *m* and *n* are the number and valency of the metal cation (M), respectively.

Several homo- and copolymers with catechol functionalities were synthesized (Scheme 1a, synthesis and characterization details given in the Supporting Information), in which catechol pendants serve dual functions of both the active material (*o*-quinone/catecholato redox couple) and the binder

Published in: ACS Applied Energy Materials (2019), vol. 2, n°5, pp. 3035-3041
DOI: 10.1021/acsaem.9b00443
Status: Postprint (Author's version)

(mussel-inspired adhesion onto carbon nanotube/carbon paper current collector via their well-known π–π interactions). (8,17,20,21) The RAPs were dispersed with multiwalled carbon nanotubes (CNTs; 1/1 (w/w)) in a solution-based process, followed by uniform deposition on glassy carbon or carbon paper current collector (see Supporting Information for electrochemical methods) for further electrochemical characterization. Note that, with these RAPs being electrically insulating, a substantial amount of conducting additive (50 wt % CNTs in this study) is required to provide sufficient electronic wiring in the electrode. (19)

Scheme 1. Tunable Electrochemical Performance via (a) Macromolecular Engineering of Catechol-Based RAPs Including Theoretical Capacity Values, and (b) Universality of P(DA_{70}-*stat*-SSA_{30}) To Reversibly Coordinate/Uncoordinate Various Cations

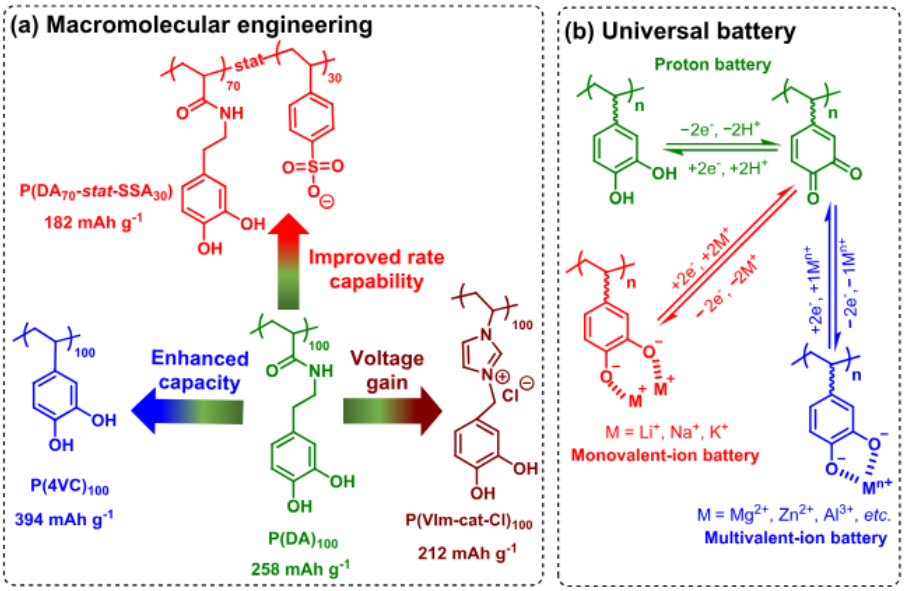

First, taking H^+ (1 M H_2SO_4; pH ≈ 0) as a representative charge carrier, we show that the macromolecular engineering is a powerful tool to precisely tune and optimize the electrochemical behavior and performances of the catechol-based RAPs. Poly(dopamine acrylamide) ($P(DA)_{100}$) (24) exhibits a reversible capacity of 190 mAh g^{-1}, whereas if DA repeating units are substituted by 4-vinylcatechol (4VC), a smaller structural redox unit, the resultant $P(4VC)_{100}$ delivered a much higher specific capacity of 330 mAh g^{-1} (Figure 1a). (21) Additionally, voltage output of the battery could be improved by attaching redox-active catechol pendants to an electron-withdrawing poly(vinylimidazolium chloride) ($P(VIm\text{-}cat\text{-}Cl)_{100}$), (25) thereby boosting redox potentials by at least +110 mV compared to the same redox-active groups confined to a neutral polymer backbone of poly(acrylamide) (Figures 1b and S3). (21) Furthermore, P(DA_{70}-*stat*-SSA_{30}) copolymer containing non-redox-active 4-styrenesulfonic acid (SSA) units exhibits superior rate capabilities compared to the homopolymer ($P(DA)_{100}$), although its specific capacity at 1C was lower (170 vs 190 mAh g^{-1}; Figure, 1c, S4, and S5). For instance, $P(DA)_{100}$ delivered 85 vs 112 mAh g^{-1} for P(DA_{70}-*stat*-SSA_{30}) at 300C that corresponds to 45 vs 66% capacity retention, respectively (Figures 1c and S4). This improved rate capability is due to SSA-mediated enhanced proton conductivity. (26) We have chosen polymer with DA/SSA = 70/30 co-monomer composition for the trade-off between the specific capacity (given by DA) and the rate capability (given by SSA).

Published in: ACS Applied Energy Materials (2019), vol. 2, n°5, pp. 3035-3041
DOI: 10.1021/acsaem.9b00443
Status: Postprint (Author's version)

Figure 1. Electrochemical performance tunability via macromolecular engineering of redox-active catechol pendants in 1 M H^+ (pH ≈ 0): (a, b) galvanostatic capacity–voltage profiles of $P(DA)_{100}$ and $P(4VC)_{100}$ (a) and $P(DA)_{100}$ and $P(VIm\text{-}cat\text{-}Cl)_{100}$ (b) at 1C, and (c) discharge capacity vs cycle number for $P(DA)_{100}$ and $P(DA_{70}\text{-}stat\text{-}SSA_{30})$ at different C-rates. 1C = 258, 394, 212, and 182 mA g^{-1}, respectively, for $P(DA)_{100}$, $P(4VC)_{100}$, $P(VIm\text{-}cat\text{-}Cl)_{100}$ and $P(DA_{70}\text{-}stat\text{-}SSA_{30})$. WE = RAP/CNTs deposited on glassy carbon (in panels a and b) and on carbon paper (in panel c); RE = Ag/AgCl; and CE = platinum wire (in panels a and b) and activated carbon (in panel c).

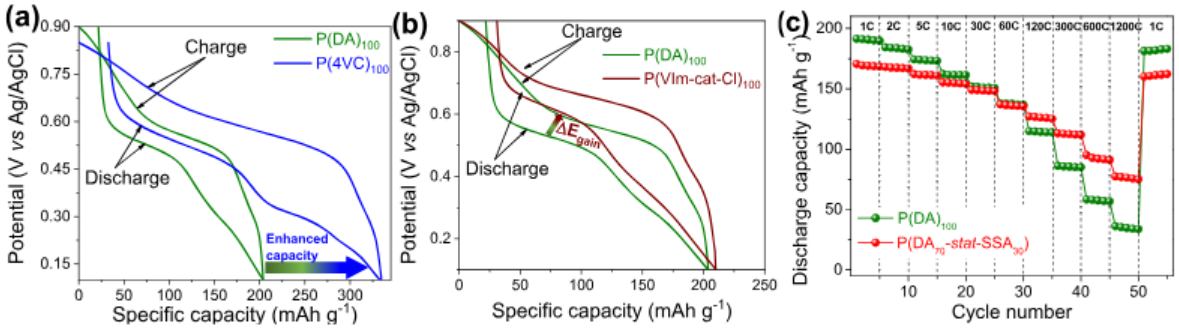

We also carried out cycling tests for $P(DA_{70}\text{-}stat\text{-}SSA_{30})$ in 1 M H^+ that demonstrated an unprecedented cycling stability, retaining 92 and 91% of its initial capacity over 1500 and 32300 cycles at 10C and 30C, respectively (Figure S6). Due to the superior electrochemical performance of $P(DA_{70}\text{-}stat\text{-}SSA_{30})$, high capacity, excellent rate capability, and ultralong cyclability, this copolymer was selected as a representative material in the following experiments.

Second, the electrochemistry of $P(DA_{70}\text{-}stat\text{-}SSA_{30})$ in a series of Britton–Robinson aqueous universal buffer solutions, pH = 1–8, by CV was carried out. For 1 < pH < 8, the redox potential of the polymer shows a systematic dependence with pH (Figure 2a) ranging from 0.1 to 0.55 V. The formal potential ($E^{0\prime}$) ascribed to the catechol/*o*-quinone redox couple decreases by ≈60 mV/pH unit increment, close to the 59 mV/pH unit expected for proton coupled redox reactions with a one-to-one stoichiometry between electrons and protons (Figure S7). (27) Therefore, it was confirmed that catechol units in $P(DA_{70}\text{-}stat\text{-}SSA_{30})$ participate in $-2e^-/-2H^+$ oxidation processes to form *o*-quinones via intermediates that are stabilized by semiquinones (Scheme 1b).

Figure 2. Universality of $P(DA_{70}\text{-}stat\text{-}SSA_{30})$ in aqueous electrolytes containing H^+, Li^+, Zn^{2+}, and Al^{3+} as charge carriers: CVs at 25 mV s^{-1} in (a) a series of Britton–Robinson universal buffer solutions, pH = 1–8, and (b) 1 M electrolyte solutions containing Li^+, Zn^{2+}, and Al^{3+}. WE = $P(DA_{70}\text{-}stat\text{-}SSA_{30})$/CNTs deposited on glassy carbon; RE = Ag/AgCl; and CE = platinum wire.

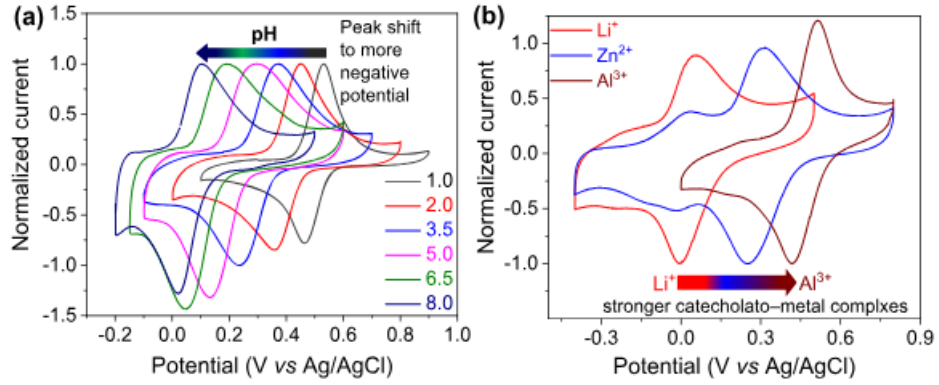

Electrochemistry of $P(DA_{70}\text{-}stat\text{-}SSA_{30})$ was then investigated in near neutral aqueous electrolytes (pH ≈ 6–7) containing monovalent cations as charge carriers (Li^+, Na^+, and K^+ from their 1 M aqueous sulfate solutions). The signature of CVs was similar in these electrolyte solutions, exhibiting a pair of clear redox peaks centered at ≈0.01 V vs Ag/AgCl (Figure S8b,d,f). Additionally, $P(DA_{70}\text{-}stat\text{-}SSA_{30})$ was also

Published in: ACS Applied Energy Materials (2019), vol. 2, n°5, pp. 3035-3041
DOI: 10.1021/acsaem.9b00443
Status: Postprint (Author's version)

found to be redox-active in mildly acidic aqueous electrolytes containing 1 M divalent (Zn^{2+}, Mg^{2+}, and Ca^{2+} respectively, from their 1 M $ZnSO_4$, $Mg(NO_3)_2$, and $Ca(NO_3)_2$ aqueous solutions; Figure S9b,d,f) and trivalent (Al^{3+}, Ce^{3+}, and Fe^{3+} from their 1 M aqueous nitrate solutions; Figure S10b,d,f) cations but with redox potentials shifted toward more positive values. Notably, as the concentrations of Li^+, Zn^{2+}, and Al^{3+} in the electrolytes increase, the cathodic peak potentials increase linearly with a positive slope (Figure S11). This is typically a Nernst-type behavior, where the cathodic peak potential ($E_{cathode}$) demonstrated linear dependency on the activity of the electrolyte cation ($a_M{}^{n+}$): (28)

$$E_{cathode} = E^0 - (0.059/n)\log a_M{}^{n+}$$

That is, the reduction of *o*-quinones preferably occurs through M^{n+} coordination, inferring that the redox reactions proceed via the coordination/uncoordination of designated cations and not with H^+ (Scheme 1b).

These results reveal several interesting features: (i) redox-active catechol pendants serve as hosts to reversibly accommodate/release both mono- and multivalent cations, including protons based on a simple catecholato–cation ($Cat^{2-}(mM^{n+})$) charge storage mechanism and, thus, can be used as the universal electrode in different H^+, Li-ion, and post-Li-ion battery technologies (Scheme 1b); (ii) the potentials corresponding to the $Cat^{2-}(mM^{n+})$/*o*-quinone couple were dramatically shifted positive ($M^+ < M^{2+} < M^{3+}$), typically by hundreds of millivolts, in the same order of electroneutralizing cation valences (Figure 2b and Table 1); and (iii) peak-to-peak voltage separation at 25 mV s^{-1} gradually increased from ≈0.06 to ≈0.1 V ($M^+ < M^{2+} < M^{3+}$; Figure 2b and Table 1) upon binding cations of higher valences, indicating sluggish kinetics in the same order (vide infra). It should be reemphasized that the underlying electrochemical reaction, mainly reduction of the $Cat^{-}(mM^{n+})$ remains the same, and the observed difference in electrochemical behavior is ascribed to the differences in electroneutralizing cation's polarizing power and the concomitant differences in strength of $Cat^{2-}(mM^{n+})$ ionic interactions.

Table 1. Electrochemical and Modeling Parameters for P(DA_{70}-*stat*-SSA_{30}) in 1 M Aqueous Electrolyte Containing Different Charge Carriers

cation	$E^{0\prime}$ (V)[a]	ΔE_p (V)[b]	$E_{red,exp}$ (V)[c]	$E_{red,calc}$ (V)[d]	E_{bind} (kcal/mol)[d]	E_{div} (>V s^{-1})[e]	k^0 (s^{-1})[f]	R_{ct} (Ω)[g]	$D_{app} \times 10^{-12}$ (cm^2 s^{-1})[h]
Li^+	0.02	0.06	0	−0.06	−7.3	0.500	56	89	17.5
Na^+	0.04	0.06	0.01			0.250	26	–	–
K^+	0.03	0.06	0			0.250	23	–	–
Zn^{2+}	0.28	0.07	0.25	0.17	−25.2	0.250	26	18.7	7.83
Mg^{2+}	0.15	0.08	0.1			0.250	21	–	–
Ca^{2+}	0.15	0.08	0.11			0.100	9.2	–	–
Al^{3+}	0.47	0.10	0.42	0.69	−49.0	0.020	1	9.6	4.8
Ce^{3+}	0.39	0.09	0.35			0.025	3	–	–
Fe^{3+}	0.49	0.25	0.36			<0.005	–	–	–

[a]$E_{anode} + E_{cathode}/2$ at 25 mV s^{-1}.[b]$E_{anode} - E_{cathode}$ at 25 mV s^{-1}.[c]$E_{red,exp}$ obtained experimentally at 25 mV s^{-1}.[d]Refer to the ESI to see the full details of the computational method to calculate $E_{red,calc}$ and E_{bind}. All of the potentials (in CV and calculated) are referenced against Ag/AgCl.[e]Scan rate above which both the anodic and cathodic branches of peak potentials diverge (see Figures S8–S10).[f]Determined by Laviron method. Note that the Laviron formalism was applied to thin electrode film (thickness in the low-micrometer range) deposited on glass carbon electrodes and, thus, cannot be compared directly with much thicker conventional battery electrodes.[g]Calculated using the equivalent circuit model shown in Figure S13c.[h]Calculated using eq S7.

Quantum-chemical calculations based on density functional theory (DFT) were performed to get additional insights into the electronic structure of the $Cat^{2-}(mM^{n+})$/*o*-quinone redox couple (refer to the Supporting Information for a detailed description of the computational methodology). All calculations are carried out in aqueous phase containing Li^+, Zn^{2+}, and Al^{3+} charge carriers as

Published in: ACS Applied Energy Materials (2019), vol. 2, n°5, pp. 3035-3041
DOI: 10.1021/acsaem.9b00443
Status: Postprint (Author's version)

representative examples from the mono-, di-, and trivalent cation families. Explicit water molecules are added to the first coordination sphere of the metal cations. Table 1 presents the experimental and the calculated reduction potentials for *o*-quinone in the presence of different metal cations. Noticeably, there is a good correlation with our experimental results, where the reduction potentials increased in the order of $Li^+ < Zn^{2+} < Al^{3+}$. The binding free energy per cation (E_{bind}) is a quantitative measure of the ionic interaction between the catecholato in the polymer and the cation upon electrochemical reduction. The estimated E_{bind} between Li^+, Zn^{2+}, and Al^{3+} and catecholato were −7.3, −25.2, and −49.0 kcal/mol per cation, respectively. Therefore, larger positive shifts in reduction potentials are associated with the higher E_{bind} due to the thermodynamic stabilization of the reduced species through the $Cat^{2-}(mM^{n+})$ complexes formation in the aforementioned order. Consequently, reoxidation of $Cat^{2-}(mM^{n+})$ to *o*-quinone becomes increasingly difficult (occurs at more positive potential) in the $Li^+ < Zn^{2+} < Al^{3+}$ order, which is also corroborated by the computed energy of the highest occupied molecular orbital (HOMO) of the $Cat^{2-}(mM^{n+})$ complexes: more negative HOMO energies, higher oxidation potential (Figure S12a). Thus, the $Cat^{2-}(mM^{n+})$/*o*-quinone charge storage mechanism offers a promising paradigm toward the design of universal organic electrodes with tunable cell voltages without modifying the molecular structure of the catechol redox core.

It has been demonstrated that the overall electrochemistry of the $Cat^{2-}(mM^{n+})$/*o*-quinone redox couple is dictated by the stabilization of catecholato by different cations. In order to understand the effect of the nature of $Cat^{2-}(mM^{n+})$ complexes on electrode dynamics, we carried out kinetic analysis of P(DA_{70}-*stat*-SSA_{30}) by CV, electrochemical impedance spectroscopy (EIS), and galvanostatic charge–discharge (GCD) experiments in aqueous electrolytes containing mono-, di-, and trivalent charge carriers (Li^+, Zn^{2+}, and Al^{3+}, respectively). Most often, the kinetics of a solid-state composite battery electrode is determined by three major parameters: (i) electrochemical reaction rate of the redox sites; (ii) charge transfer at the electrode–electrolyte interface; and (iii) solid-state ion transport in the bulk. (29) Thus, we have investigated these parameters to understand the origin of marked electrochemical behavior differences of P(DA_{70}-*stat*-SSA_{30}) in the tested electrolytes.

First, the CVs of P(DA_{70}-*stat*-SSA_{30}) in different electrolytes were characterized by slightly larger peak-to-peak voltage separations in the $Li^+ < Zn^{2+} < Al^{3+}$ trend (Figure 2b and Table 1), suggesting faster kinetics in the opposite order. Furthermore, from the scan rate dependence of the peak potentials experiments, it is evident that the oxidative and reductive peak potentials diverge (E_{div}) above 0.50, 0.25, and 0.02 V s^{-1}, respectively, in Li^+, Zn^{2+}, and Al^{3+} containing electrolytes (Figures S8a,b; S9a,b; and S10a,b and Table 1), indicating facilitated faradic charge transfer kinetics in $Li^+ > Zn^{2+} > Al^{3+}$ order. Additionally, apparent rate constants (k^0), being a quantitative measure of redox kinetics, were determined by Laviron formalism and found to be 56 and 26 times higher in Li^+ and Zn^{2+}, respectively, compared to that in Al^{3+} (Table 1). (30)

Second, the kinetic aspects of electro-ionic reactions in P(DA_{70}-*stat*-SSA_{30}) were probed with EIS technique. Figure S13a shows the resultant Nyquist plots with two well-defined regions, a depressed single semicircle in the high-to-mid-frequency region and an inclined line in the low-frequency region, often connected by Warburg impedance (σ_w), represented by a line of ∼45° slope. (20) The obtained EIS parameters were simulated and fitted with an equivalent circuit model as represented in Figure S13c. Charge transfer resistance, R_{ct} (9.6 < 18.7 < 89 Ω, Table 1), which accounts for the interfacial

Published in: ACS Applied Energy Materials (2019), vol. 2, n°5, pp. 3035-3041
DOI: 10.1021/acsaem.9b00443
Status: Postprint (Author's version)

cation intake from the electrolyte, followed $Al^{3+} < Zn^{2+} < Li^{+}$ trend, suggesting facile charge transfer reactions in the opposite direction.

Finally, the Nyquist profile of P(DA_{70}-*stat*-SSA_{30}) featured an increasing Warburg diffusion region (Z_w) in $Li^{+} < Zn^{2+} < Al^{3+}$ order, and the associated coefficient σ_w (14.3 < 21.4 < 27.1 Ω $s^{-1/2}$, Figure S13b) values were in the same order as Z_w (Figure S13a). Consequently, the calculated apparent diffusion coefficient (D_{app}) for P(DA_{70}-*stat*-SSA_{30}) in Li^{+} and Zn^{2+} containing electrolytes was found to be, respectively, about 4- and 2-fold higher than that in Al^{3+}, inferring superior ion diffusion properties in the $Li^{+} > Zn^{2+} > Al^{3+}$ order (Table 1). This ion mobility trend is once again supplemented by the calculated lower (less negative) E_{bind} values in the same order: weaker electrostatic interactions between the host and the metal cation imply a faster ion mobility in the bulk.

Figure 3a shows discharge capacities of P(DA_{70}-*stat*-SSA_{30}) with respect to cycle number by GCD experiments in a Swagelok-T half-cell at progressively increasing C-rates. The representative capacity–potential profiles are given in Figure S14. It is also apparent from these potential profiles that the charge/discharge plateaus corresponding to the reversible redox dissociation/formation of Cat^{2-} (mM^{n+}) complexes were shifted to higher values in the order $Li^{+} < Zn^{2+} < Al^{3+}$, despite their sloping nature, which is in good agreement with CV experiments and DFT calculations. P(DA_{70}-*stat*-SSA_{30}) delivered reversible capacities in the range of 130–140 mAh g^{-1} in Li^{+}, Zn^{2+}, and Al^{3+} containing aqueous electrolytes at 1C. With increasing C-rates, both the capacities and consequently their capacity retentions (capacities at higher C-rates wrt the capacity at 1C) decreased monotonically in $Li^{+} < Zn^{2+} < Al^{3+}$ order. For instance, the discharge capacities (and their percent retentions) were 77 (59%), 67 (49%), and 47 (33%) mAh g^{-1} at 120C, respectively, in Li^{+}, Zn^{2+}, and Al^{3+} containing aqueous electrolytes (Figures 3a and S14d). It is remarkable that when the C-rate was brought back to 1C, nearly quantitative capacity recovery was observed in all of the cases, discarding irreversible capacity fade during the high-C-rate runs. The combined CV, EIS, and GCD experiments and computational studies reveal that P(DA_{70}-*stat*-SSA_{30}) exhibited facilitated faradic charge transfer kinetics and enhanced ion mobilities in the order of $Li^{+} > Zn^{2+} > Al^{3+}$ (Table 1), consequently, delivering superior dynamic performances in the aforementioned order.

Figure 3. Electrochemical performance of P(DA_{70}-*stat*-SSA_{30}) in the aqueous electrolytes containing different charge carriers at 1 M concentration: (a) comparative rate capability studies depicting discharge capacity vs cycle number and (b) ultralong cycling tests in a coin cell configuration at 30C. WE = P(DA_{70}-*stat*-SSA_{30})/CNTs deposited on carbon paper; RE = Ag/AgCl; and CE = activated carbon.

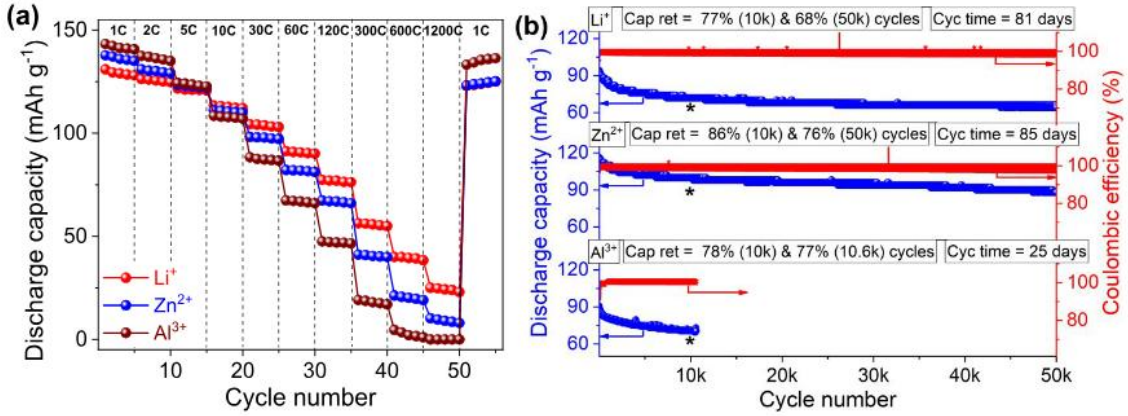

Published in: ACS Applied Energy Materials (2019), vol. 2, n°5, pp. 3035-3041
DOI: 10.1021/acsaem.9b00443
Status: Postprint (Author's version)

Electrochemical stability of the redox centers is another crucial requisite for the development of long-cycling batteries. Thus, we evaluated the medium- and long-term cyclability of P(DA_{70}-*stat*-SSA_{30}) by repeated GCD experiments both in Swagelok-T and coin cell configurations. The polymer attained stable capacities of 133, 132, and 130 mAh g^{-1}, respectively, Li^+, Zn^{2+}, and Al^{3+} containing electrolytes, and retained 86, 87, and 84% of their initial capacities over 1500 repeated full charge–discharge cycles at 10C (Figure S15). The P(DA_{70}-*stat*-SSA_{30}) assembled in a two-electrode hybrid full-cell configuration (overcapacitive carbon|polymer cell) also delivered an impressive ultralong cyclability, retaining 77, 86, and 78% of their initial capacities over a prolonged 10000 cycles at 30C in Li^+, Zn^{2+}, and Al^{3+} electrolytes, respectively (Figures 3b and S16). Further extending the cycling to 50000 cycles resulted in small capacity losses of 32 and 24%, respectively, in Li^+ and Zn^{2+} electrolytes. However, after 10000 cycles the capacity in Al^{3+} containing electrolyte decreased drastically probably due to the accumulation of trivalent cations at the catechol reaction sites, which form stronger complexes with trivalent cations. This might reduce their redox activity and hence deteriorate the cycling performance in ultralong-term cycling experiments. Notably, the average Coulombic efficiencies in all of the cycling tests remained more than 99%. It is worth mentioning here that the main purpose of using this hybrid cell is not to assemble a practical battery (voltage output would be too low; less than 1 V) but to investigate the electrochemical properties of polycatechols.

In summary, we have demonstrated that a simple and stable catecholato–cation (Cat^{2-}(*m*M^{n+})) charge storage mechanism offers a unique platform to employ catechol-based RAPs as universal electrode materials for H^+, Li-ion, and post-Li-ion (mono-, di-, and trivalent) batteries. Interestingly, the overall electrochemical performances of the electrodes were dictated by the strength of the Cat^{2-}(*m*M^{n+}) interactions: the stronger the complexes ($M^+ < M^{2+} < M^{3+}$) and the higher the formal redox potentials, adversely, the slower the kinetics as revealed by the combined CV, EIS, GCD, and computational studies. The gains in the redox potentials for the P(DA_{70}-*stat*-SSA_{30}) by +260 and +450 mV upon binding Zn^{2+} and Al^{3+}, respectively, compared to Li^+ were truly profound; consequently, the battery would exhibit a much higher cell voltage and, thus, energy density in these configurations, without modifying the molecular structure of the catechol redox core. Additionally, P(DA_{70}-*stat*-SSA_{30}) has also shown excellent cycling stabilities in all of the tested electrolyte systems. We postulate that the combination of catechol-based universal polymeric electrodes capable of hosting a multitude of charge carriers and aqueous electrolyte systems may open new horizons to develop numerous Li- and post-Li-ion next-generation high-performance, safe, and sustainable water-based rechargeable batteries. Current works deal with assembling, optimizing, and electrochemical testing of various multivalent batteries.

ASSOCIATED CONTENT

Supporting Information

The Supporting Information is available free of charge on the ACS Publications website at DOI: 10.1021/acsaem.9b00443.

- Materials; P(DA_{70}-*stat*-SSA_{30}) synthesis details (Scheme S1, Figures S1 and S2, and Tables S1 and S2); electrode fabrication and cell assembly; characterization techniques; electrochemical

Published in: ACS Applied Energy Materials (2019), vol. 2, n°5, pp. 3035-3041
DOI: 10.1021/acsaem.9b00443
Status: Postprint (Author's version)

analysis; materials' and batteries' electrochemical performance (Figures S3–S11 and S13–S16); computational procedure; DFT-computed HOMO energy levels(Figure S12); and computed species' Cartesian coordinates (PDF)

AUTHOR INFORMATION

Corresponding Author

*Tel.: 0034917371131. E-mail: rebeca.marcilla@imdea.org.

ORCID

Nagaraj Patil: 0000-0002-2873-6824

Andreas Mavrandonakis: 0000-0002-5053-8154

Christine Jérôme: 0000-0001-8442-5740

Christophe Detrembleur: 0000-0001-7849-6796

Rebeca Marcilla: 0000-0002-5660-6381

Notes

The authors declare no competing financial interest.

ACKNOWLEDGMENTS

We thank the Spanish MINECO (formerly MICINN) through the MAT2015-64167-C2-1-R project, the "Fonds de la Recherche Scientifique" (FRS-FNRS, Belgium), and the TALENTO grant (2017-T1/AMB-5264) from Comunidad de Madrid for financial support. We acknowledge the computing facilities of CSUC for providing resources that contributed to the research results reported within this paper. C.D. is FRS-FNRS Research Director.

REFERENCES

(1) Kim, H.; Hong, J.; Park, K.-Y.; Kim, H.; Kim, S.-W.; Kang, K. Aqueous Rechargeable Li and Na Ion Batteries. Chem. Rev. 2014, 114, 11788−11827.

(2) Canepa, P.; Sai Gautam, G.; Hannah, D. C.; Malik, R.; Liu, M.; Gallagher, K. G.; Persson, K. A.; Ceder, G. Odyssey of Multivalent Cathode Materials: Open Questions and Future Challenges. Chem. Rev. 2017, 117, 4287−4341.

(3) Huang, J.; Guo, Z.; Ma, Y.; Bin, D.; Wang, Y.; Xia, Y. Recent Progress of Rechargeable Batteries Using Mild Aqueous Electrolytes. Small Methods 2019, 3, 1800272.

Published in: ACS Applied Energy Materials (2019), vol. 2, n°5, pp. 3035-3041
DOI: 10.1021/acsaem.9b00443
Status: Postprint (Author's version)

(4) Yang, Z.; Zhang, J.; Kintner-Meyer, M. C. W.; Lu, X.; Choi, D.; Lemmon, J. P.; Liu, J. Electrochemical Energy Storage for Green Grid. Chem. Rev. 2011, 111, 3577−3613.

(5) Armand, M.; Tarascon, J.-M. Building Better Batteries. Nature 2008, 451, 652−657.

(6) Nishide, H.; Oyaizu, K. Toward Flexible Batteries. Science 2008, 319, 737−738.

(7) Muench, S.; Wild, A.; Friebe, C.; Haupler, B.; Janoschka, T.; Schubert, U. S. Polymer-Based Organic Batteries. Chem. Rev. 2016, 116, 9438−9484.

(8) Patil, N.; Jérôme, C.; Detrembleur, C. Recent Advances in the Synthesis of Catechol-Derived (Bio)Polymers for Applications in Energy Storage and Environment. Prog. Polym. Sci. 2018, 82, 34−91.

(9) Lee, S.; Kwon, G.; Ku, K.; Yoon, K.; Jung, S.-K.; Lim, H.-D.; Kang, K. Recent Progress in Organic Electrodes for Li and Na Rechargeable Batteries. Adv. Mater. 2018, 30, 1704682.

(10) Lu, Y.; Zhang, Q.; Li, L.; Niu, Z.; Chen, J. Design Strategies toward Enhancing the Performance of Organic Electrode Materials in Metal-Ion Batteries. Chem. 2018, 4, 2786−2813.

(11) Häupler, B.; Wild, A.; Schubert, U. S. Carbonyls: Powerful Organic Materials for Secondary Batteries. Adv. Energy Mater. 2015, 5, 1402034.

(12) Gheytani, S.; Liang, Y.; Wu, F.; Jing, Y.; Dong, H.; Rao, K. K.; Chi, X.; Fang, F.; Yao, Y. An Aqueous Ca-Ion Battery. Adv. Sci. 2017, 4, 1700465.

(13) Liang, Y.; Jing, Y.; Gheytani, S.; Lee, K.-Y.; Liu, P.; Facchetti, A.; Yao, Y. Universal Quinone Electrodes for Long Cycle Life Aqueous Rechargeable Batteries. Nat. Mater. 2017, 16, 841−848.

(14) Fan, X.; Wang, F.; Ji, X.; Wang, R.; Gao, T.; Hou, S.; Chen, J.; Deng, T.; Li, X.; Chen, L.; et al. A Universal Organic Cathode for Ultrafast Lithium and Multivalent Metal Batteries. Angew. Chem., Int. Ed. 2018, 57, 7146−7150.

(15) Hernández-Burgos, K.; Rodríguez-Calero, G. G.; Zhou, W.; Burkhardt, S. E.; Abruña, H. D. Increasing the Gravimetric Energy Density of Organic Based Secondary Battery Cathodes Using Small Radius Cations (Li+ and Mg2+). J. Am. Chem. Soc. 2013, 135, 14532− 14535.

(16) Kim, Y. J. o.; Wu, W.; Chun, S.-E.; Whitacre, J. F.; Bettinger, C. J. Catechol-Mediated Reversible Binding of Multivalent Cations in Eumelanin Half-Cells. Adv. Mater. 2014, 26, 6572−6579.

(17) Liu, T.; Kim, K. C.; Lee, B.; Chen, Z.; Noda, S.; Jang, S. S.; Lee, S. W. Self-Polymerized Dopamine as an Organic Cathode for Li- and Na-Ion Batteries. Energy Environ. Sci. 2017, 10, 205−215.

(18) Kim, D. J.; Yoo, D.-J.; Otley, M. T.; Prokofjevs, A.; Pezzato, C.; Owczarek, M.; Lee, S. J.; Choi, J. W.; Stoddart, J. F. Rechargeable Aluminium Organic Batteries. Nat. Energy 2019, 4, 51−59.

(19) Nokami, T.; Matsuo, T.; Inatomi, Y.; Hojo, N.; Tsukagoshi, T.; Yoshizawa, H.; Shimizu, A.; Kuramoto, H.; Komae, K.; Tsuyama, H.; et al. Polymer-Bound Pyrene-4,5,9,10-Tetraone for Fast-Charge and -Discharge Lithium-Ion Batteries with High Capacity. J. Am. Chem. Soc. 2012, 134, 19694−19700.

(20) Patil, N.; Aqil, A.; Ouhib, F.; Admassie, S.; Inganas, O.; Jérôme, C.; Detrembleur, C. Bioinspired Redox-Active Catechol-Bearing Polymers as Ultrarobust Organic Cathodes for Lithium Storage. Adv. Mater. 2017, 29, 1703373.

Published in: ACS Applied Energy Materials (2019), vol. 2, n°5, pp. 3035-3041
DOI: 10.1021/acsaem.9b00443
Status: Postprint (Author's version)

(21) Patil, N.; Aqil, M.; Aqil, A.; Ouhib, F.; Marcilla, R.; Minoia, A.; Lazzaroni, R.; Jérôme, C.; Detrembleur, C. Integration of Redox-Active Catechol Pendants into Poly(Ionic Liquid) for the Design of High-Performance Lithium-Ion Battery Cathodes. Chem. Mater. 2018, 30, 5831−5835.

(22) Milczarek, G.; Inganas, O. Renewable Cathode Materials from Biopolymer/Conjugated Polymer Interpenetrating Networks. Science 2012, 335, 1468−1471.

(23) Krogsgaard, M.; Nue, V.; Birkedal, H. Mussel-Inspired Materials: Self-Healing through Coordination Chemistry. Chem. Eur. J. 2016, 22, 844−857.

(24) Patil, N.; Falentin-Daudre, C.; Jérôme, C.; Detrembleur, C. Mussel-Inspired Protein-Repelling Ambivalent Block Copolymers: Controlled Synthesis and Characterization. Polym. Chem. 2015, 6, 2919−2933.

(25) Patil, N.; Cordella, D.; Aqil, A.; Debuigne, A.; Admassie, S.; Jérôme, C.; Detrembleur, C. Surface- and Redox-Active Multifunctional Polyphenol-Derived Poly(Ionic Liquid)s: Controlled Synthesis and Characterization. Macromolecules 2016, 49, 7676−7691.

(26) Chen, X. C.; Wong, D. T.; Yakovlev, S.; Beers, K. M.; Downing, K. H.; Balsara, N. P. Effect of Morphology of Nanoscale Hydrated Channels on Proton Conductivity in Block Copolymer Electrolyte Membranes. Nano Lett. 2014, 14, 4058−4064.

(27) Lin, Q.; Li, Q.; Batchelor-McAuley, C.; Compton, R. G. Two-Electron, Two-Proton Oxidation of Catechol: Kinetics and Apparent Catalysis. J. Phys. Chem. C 2015, 119, 1489−1495.

(28) Jayalakshmi, M.; Mohan Rao, M.; Scholz, F. Electrochemical Behavior of Solid Lithium Manganate (LiMn2O4) in Aqueous Neutral Electrolyte Solutions. Langmuir 2003, 19, 8403−8408.

(29) Zhang, H.; Yu, X.; Braun, P. V. Three-Dimensional Bicontinuous Ultrafast-Charge and -Discharge Bulk Battery Electrodes. Nat. Nanotechnol. 2011, 6, 277−281.

(30) Sterby, M.; Emanuelsson, R.; Huang, X.; Gogoll, A.; Strømme, M.; Sjödin, M. Characterization of PEDOT-Quinone Conducting Redox Polymers for Water Based Secondary Batteries. Electrochim. Acta 2017, 235, 356−364.